

Development of a Liquid Argon Drift Chamber

Diploma Thesis

Alessandra Telleschi, Institute for Particle Physics, ETH Zuerich

under the supervision of

Prof. Dr. André Rubbia
Dr. Andreas Badertscher

October 28, 2002

Abstract

In this report the development and construction of a liquid argon (LAr) drift chamber and the measurements of the drifted electrons are described. The chamber is composed from an anode with 13 strips, a cathode and a radioactive Pb^{210} α -source, which ionizes the LAr, producing free electrons. The free electrons drift to the anode, where they are detected by the strips. The chamber is 5 cm long, and it is the first study for the construction of a longer drift chamber in which the Lorentz angle between the electron trajectory and the electric field lines, due to a magnetic field perpendicular to the electric field, is measurable.

Contents

| | | |
|----------|---|-----------|
| 1 | Introduction | 2 |
| 1.1 | The ICARUS experiment | 2 |
| 1.2 | The Lorentz angle | 3 |
| 1.3 | The drift chamber | 5 |
| 1.3.1 | Mechanics | 5 |
| 1.3.2 | The α -source | 7 |
| 2 | Design of the drift chamber | 10 |
| 2.1 | Choice of the potentials of the source and of the cathode . . . | 10 |
| 2.2 | Analytical result for the electric field | 10 |
| 2.3 | Simulation results | 12 |
| 3 | Experimental setup and measurements | 14 |
| 3.1 | Measuring setup and LAr filling procedure | 14 |
| 3.2 | Electronics | 14 |
| 3.2.1 | The high voltage | 14 |
| 3.2.2 | The signal read-out chain | 14 |
| 3.2.3 | Electronic board | 17 |
| 3.2.4 | Calibration | 17 |
| 4 | Data acquisition and analysis | 25 |
| 4.1 | Data acquisition | 25 |
| 4.2 | Data analysis | 30 |
| 5 | Results | 32 |
| 5.1 | Measurement program | 32 |
| 5.2 | Results of the measurements with 12 strips | 33 |
| 5.2.1 | The cuts | 33 |
| 5.2.2 | The results | 35 |
| 5.2.3 | Discussion of the results | 36 |
| 6 | Conclusions | 43 |

Chapter 1

Introduction

This diploma thesis is a study within the framework of the ICARUS research project.

1.1 The ICARUS experiment

The ICARUS (Imaging Cosmic And Rare Underground Signal) experiment [1, 2] will take place at the Gran Sasso National Laboratory near Rome.

The ICARUS program addresses many fundamental issues:

- The nature of the neutrinos, in particular the question of neutrino mass, through the study of atmospheric neutrinos and through long baseline studies with the foreseen CERN neutrino beam.
- The stability of the nucleon
- The study of solar neutrinos
- The detection of astrophysical and cosmological neutrinos from supernovae.

A novel liquid argon (LAr) drift chamber was developed as a particle detector. The operating principle of the ICARUS liquid argon Time Projection Chamber (TPC) is rather simple and it is sketched in Figure 1.1.

Any ionizing event from a particle interaction or decay, taking place in a volume of liquid argon, produces ion-electron pairs. The electrons that don't recombine, drift parallel to the uniform E-field and are detected from the read-out wires.

From the measurement of the signals on the wires and the measurement of the drift time, a full 3-D image of the event is provided.

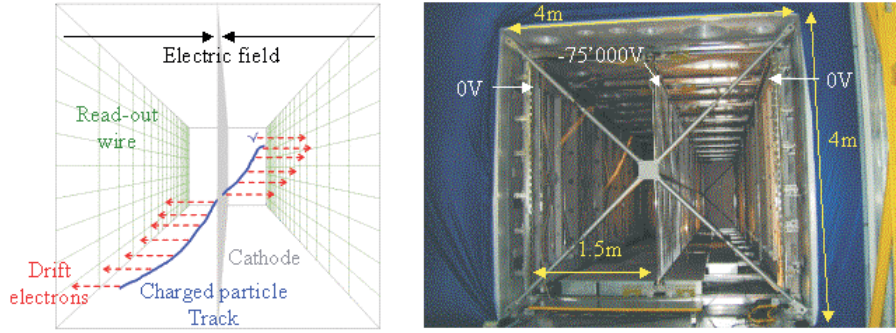


Figure 1.1: Left: Principle of the LAr TPC. Right: view into the open first ICARUS T600 half-module.

1.2 The Lorentz angle

The purpose of this diploma thesis is the development of a small LAr drift chamber in which the deviation of the electrons due to a magnetic field, perpendicular to the electric field, is measurable (Lorentz angle).

The Lorentz angle is the angle between the electrons trajectory in a static electromagnetic field and the direction of the electric field lines (see Figure 1.2).

To estimate the Lorentz angle we need first to find the mobility of electrons. The following calculations are valid for electrons in a gas; we consider them as a valid approximation for electrons in LAr.

When an electric field is applied, the electrons move along the field direction. The average of this motion is called drift velocity v_d .

The mobility of the charged particles in an electric field is defined as [3]:

$$\mu = \frac{v_d}{E} \quad (1.1)$$

Except for very low fields, the mobility of electrons is not constant in gas. In fact, due to their small mass, electrons can substantially increase their energy under the influence of an electric field.

One can approximate the drift velocity as [3]:

$$v_d = \frac{e}{2m} \cdot E \cdot \tau \quad (1.2)$$

Where τ is the mean time between collisions, in general a function of the electric field E .

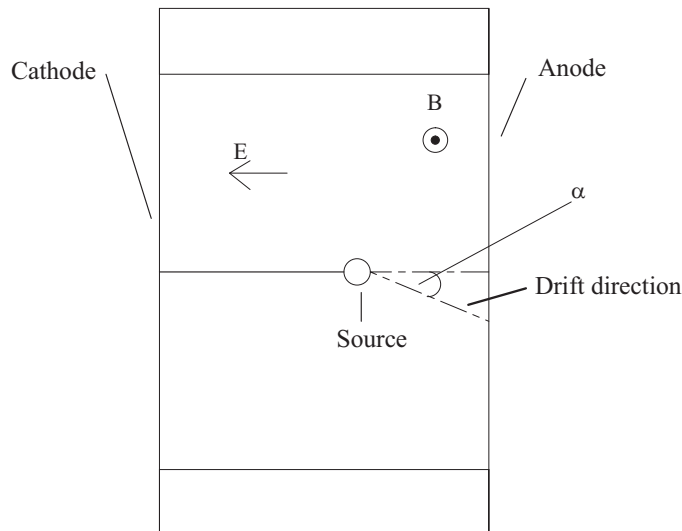


Figure 1.2: Definition of the Lorentz angle α in an electric field E and a magnetic field B .

Hence, we find for the mobility μ the following equation:

$$\mu = \frac{e}{2m} \cdot \tau \quad (1.3)$$

The presence of a magnetic field modifies the drift properties of a cloud of electrons. A Lorentz force is applied to each moving charge. As a consequence, the electrons move along a line different from an electric field line. The velocity in the presence of a magnetic field, v_{DB} is different from the drift velocity v_d . In the general case we have [4]:

$$v_{DB} = \frac{v_d}{1 + \omega^2 \tau^2} [\hat{E} + \omega \tau (\hat{E} \wedge \hat{B}) + \omega^2 \tau^2 (\hat{E} \cdot \hat{B}) \hat{B}] \quad (1.4)$$

where \hat{E} is the unit vector in the E-field direction and \hat{B} is the unit vector in the B-field direction and ω is the cyclotron frequency:

$$\omega = \frac{e \cdot B}{m}. \quad (1.5)$$

In case of a movement in a constant electric field and a perpendicular constant magnetic field, the electrons will drift along a straight line at an angle α with respect to the electric field lines (see Figure 1.2). In this case $\hat{E} \cdot \hat{B} = 0$ and the third term in equation 1.4 disappears. We obtain:

$$v_{DB} = \frac{v_d}{1 + \omega^2 \tau^2} [\hat{E} + \omega \tau (\hat{E} \wedge \hat{B})] \quad (1.6)$$

The direction of the E-field and $\hat{E} \wedge \hat{B}$ is sketched on Figure 1.3. The angle

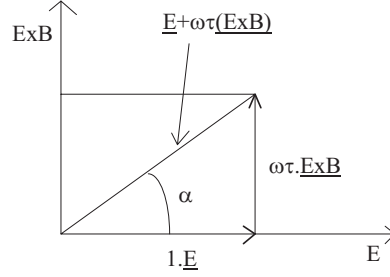


Figure 1.3: Definition of the Lorentz angle α .

α is then

$$\tan \alpha = \frac{\omega\tau}{1} \quad (1.7)$$

From equation (1.3) we obtain for τ

$$\tau = \mu \cdot \frac{2m}{e} \quad (1.8)$$

At the end we reach for the Lorentz angle:

$$\tan \alpha = \frac{e \cdot B}{m} \cdot \mu \cdot \frac{2m}{e} = 2\mu B \quad (1.9)$$

In LAr, for an electric field $E=500$ V/cm, we have a drift velocity of about 1,5 mm/ μ s [5]. The mobility of electrons is then $\mu = \frac{v_d}{E} = 300 \frac{cm^2}{V \cdot s}$. If we take for the magnetic field the value $B = 0.5 \cdot 10^{-4} \frac{V \cdot s}{cm^2}$ we obtain a Lorentz angle of

$$\alpha = 30 mrad \simeq 2^\circ. \quad (1.10)$$

1.3 The drift chamber

1.3.1 Mechanics

The principle of the drift chamber is schematically shown in Figure 1.4.

It consists of two parallel copper-plated vetronite plates: an anode and a cathode. The vetronite plates are 10cm \times 10cm wide and 1,5 mm thick. The copper layers have a size of 8cm \times 8cm.

The anode is copper plated only on one side. In the copper layer a series of 13 strips, 0.9mm wide, 30mm long, with a pitch of 1mm, were etched (see Figure 1.5). The anode and the strips are connected to ground.

The cathode is copper plated on both sides; the negative high voltage for the drift field is applied to both sides. At the center of the cathode, but electrically insulated from it, is the (conducting) holder for mounting the radioactive Pb^{210} source (see Figure 1.6).

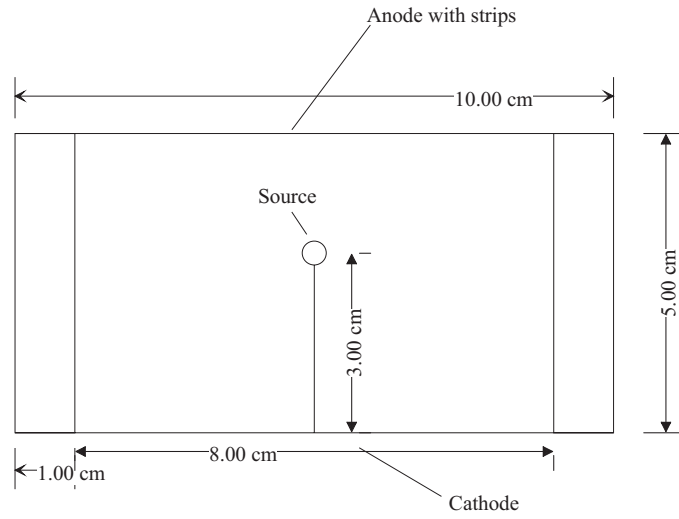


Figure 1.4: Schematic view of the drift chamber.

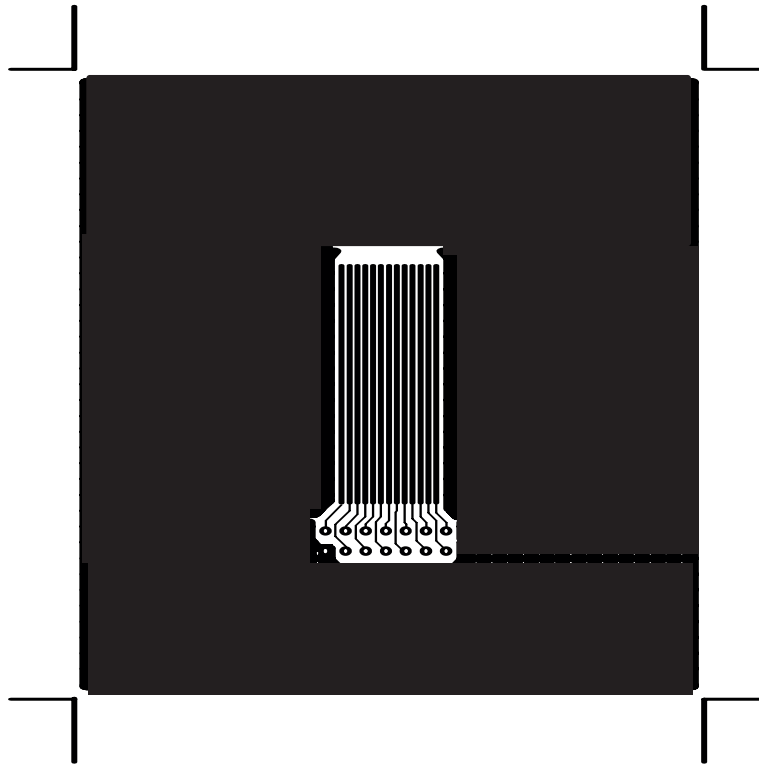


Figure 1.5: Anode with the strips.

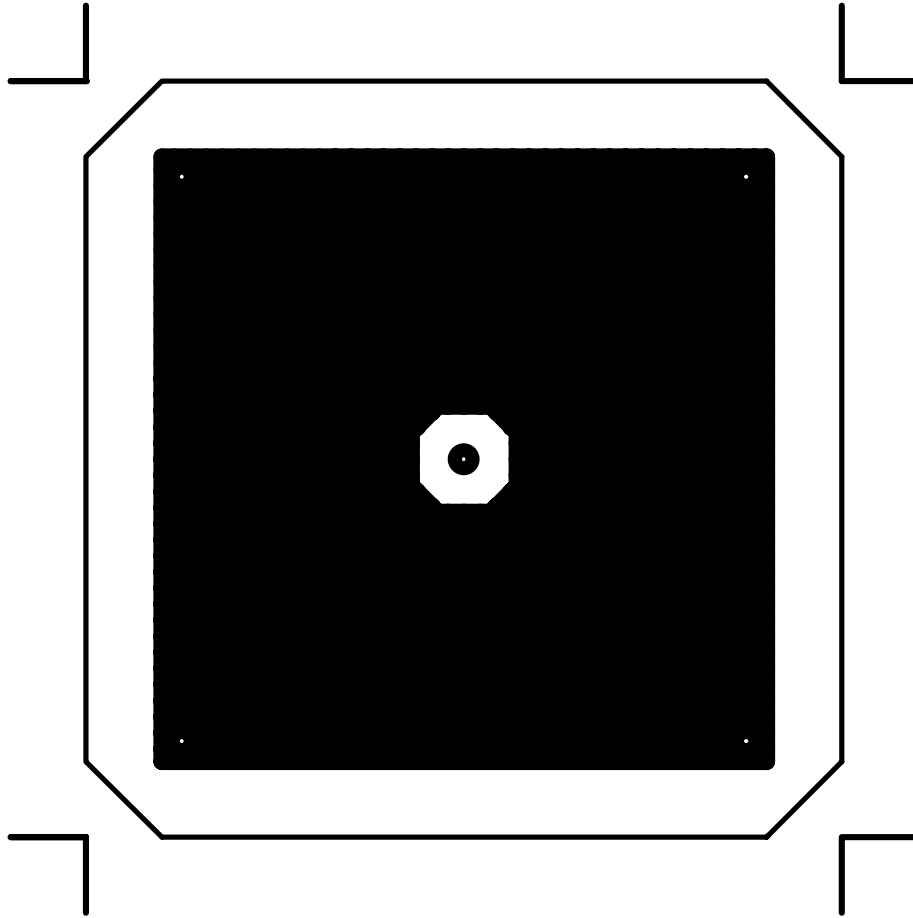


Figure 1.6: Cathode and source holder.

The distance between anode and cathode can be varied; for this study a distance of 5cm was used. The two plates are fixed together by 4 polyamide cylinders with a diameter of 1 cm fixed with polyamide screws. A radioactive Pb^{210} α -source is put between the two plates at a distance of 2cm from the anode.

The picture of the chamber is shown in Figure 1.7.

1.3.2 The α -source

The source is placed on the surface of a platinum sphere with a diameter of 0.5mm. It is connected to a very thin platinum wire of $76\mu\text{m}$ of diameter, which is connected to the source holder, at the center of the cathode plate, through a copper wire with 0.5 mm diameter.

The α -particles emitted from the source ionize the LAr and produce free



Figure 1.7: Picture of the chamber.

electrons. The ionization density for an α -particle in liquid argon is very high, but the recombination of the electrons with argon ions is high, too [5]. To suppress the recombination the spherical geometry has been chosen for the source support and a negative high voltage has to be applied to the radioactive source, in order to have an electric field on the sphere surface of 50 kV/cm at least [5].

The spherical α -source has an activity of about 10 Bq. It consists of a thin Pt wire, from which a spherical drop was melted at one end in a butane flame. On this Pt drop a thin layer of lead, containing the α -emitter ${}_{82}\text{Pb}^{210}$, was electrolytically applied at the radio-chemistry department of PSI, Villigen, Switzerland. The property of the α -emitter are shown in Table 1.1 [6].

The decay chain of ${}_{82}\text{Pb}^{210}$ is shown on Figure 1.8. As shown in the decay chain, the α -particles that we used for the ionization of LAr are those of the decay of ${}_{84}\text{Po}^{210}$ in ${}_{82}\text{Pb}^{206}$, which have an energy of 5,3MeV.

More information about the source are given in ref. [5].

| Isotope | Half-life-time | Modes of decay | Particle energy [MeV] |
|--------------------------|----------------|----------------|-----------------------|
| ${}_{82}\text{Pb}^{210}$ | 22,3y | β | 0,02 |
| | | | 0,06 |
| | | α | 3,72 |
| | | γ | 0,047 |

Table 1.1: Properties of the α -source

Spherical Pb^{210} α -Source

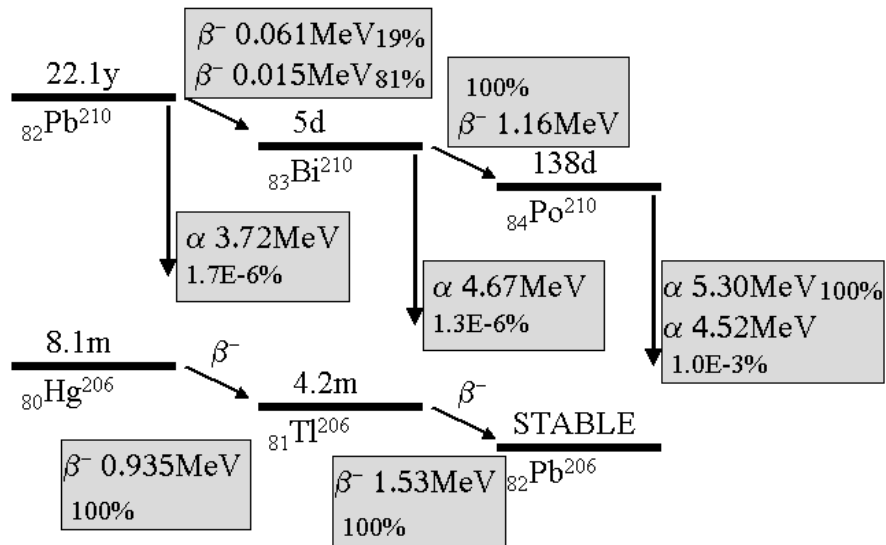


Figure 1.8: Decay chain of ${}_{82}\text{Pb}^{210}$.

Chapter 2

Design of the drift chamber

The first step for the construction of the drift chamber was the calculation and simulation of the electric field in the drift chamber.

2.1 Choice of the potentials of the source and of the cathode

The first goal is to study if the signals are measurable in such a drift chamber. For that purpose a little drift chamber, with a short drift space, has to be constructed. We planned a 5 cm long chamber with a distance between source and anode (strips) of 2 cm. In the chamber we wanted to have the same electric field as in the ICARUS detector, that is 500 Volt/cm. Thus, in a chamber of a total length of 5 cm, with the strips on ground, the cathode has to be at a potential of -2,5 kV.

It is also important to have a high electric field on the source sphere in order to suppress the recombination of the electrons with the argon ions [5]. This recombination is sufficiently suppressed when on the sphere surface the electric field is at least 50 kV/cm.

If we draw a plot of the electric potential as a function of the distance from the anode to the cathode, without source, we obtain a line. The voltage of the source in this diagram has to be below this line (see Figure 2.1).

We put the source at a distance of 3 cm from the cathode, where the potential from the two planar electrodes is -1 kV and we calculate and simulate the electric field for a source at -4 kV.

2.2 Analytical result for the electric field

The geometry of the problem is sketched in Figure 2.2. For the calculation we assume cylindrical symmetry.

The analytical formula for the electric field in the point (x,z) of the cartesian

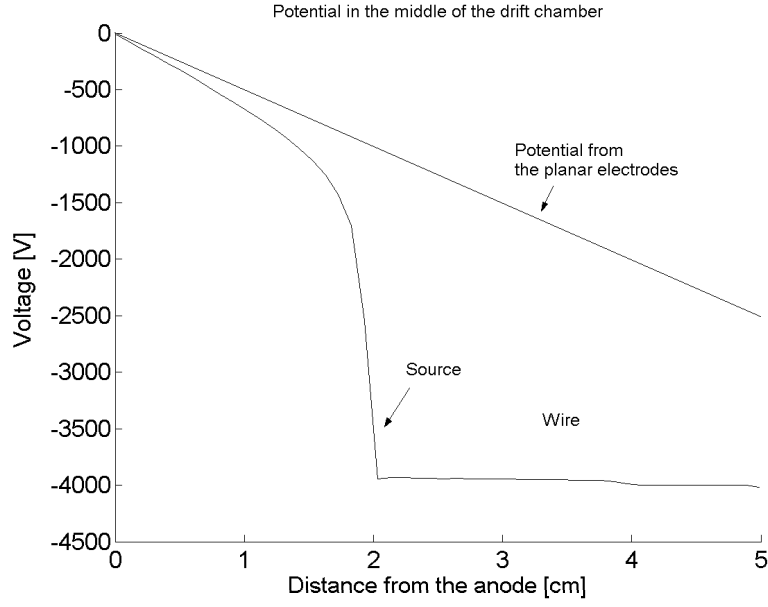


Figure 2.1: Potentials of the drift chamber and of the source.

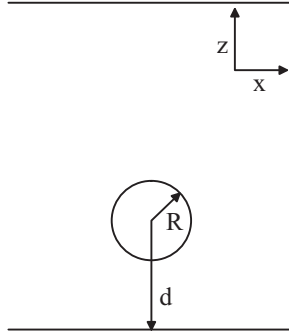


Figure 2.2: Geometry of the problem for the analytic calculations.

plane, with the origin in the center of the sphere, is [7]:

$$\begin{cases} E_x &= (V_3 - V_2 + E_0 d) \frac{R \cdot x}{(x^2 + z^2)^{3/2}} + 3E_0 \frac{R^3 \cdot x \cdot z}{(x^2 + z^2)^{5/2}} \\ E_z &= E_0 + (V_3 - V_2 + E_0 d) \frac{R \cdot z}{(x^2 + z^2)^{3/2}} + 3E_0 \frac{R^3 \cdot z^2}{(x^2 + z^2)^{5/2}} - E_0 \frac{R^3}{(x^2 + z^2)^{3/2}} \end{cases}$$

where V_3 is the potential on the source, V_2 is the potential of the cathode and E_0 is the homogeneous electric field between the cathode and the anode (without the source), that is $500V/cm$.

On the sphere surface this formula reduces to:

$$E = 3E_o + \frac{(V_3 - V_2 + E_o d)}{R} \quad (2.1)$$

If we put in this formula the values mentioned above for the drift chamber we reach an electric field on the sphere surface of 121,5 kV/cm, that is a field strong enough to suppress the recombination of the electrons with ions.

2.3 Simulation results

The electric field for the same geometry has been simulated with the simulation program Femlab, too. In this simulation, we put a voltage of -2,5kV on the cathode, -4kV on the source sphere, whereas the anode with the strips is on ground. With a cylindrical geometry the equipotential lines represented in Figure 2.3 and Figure 2.4 have been obtained. The equipotential lines in these two figures are drawn on a plane perpendicular to the anode and cathode planes, in the center of the drift chamber.

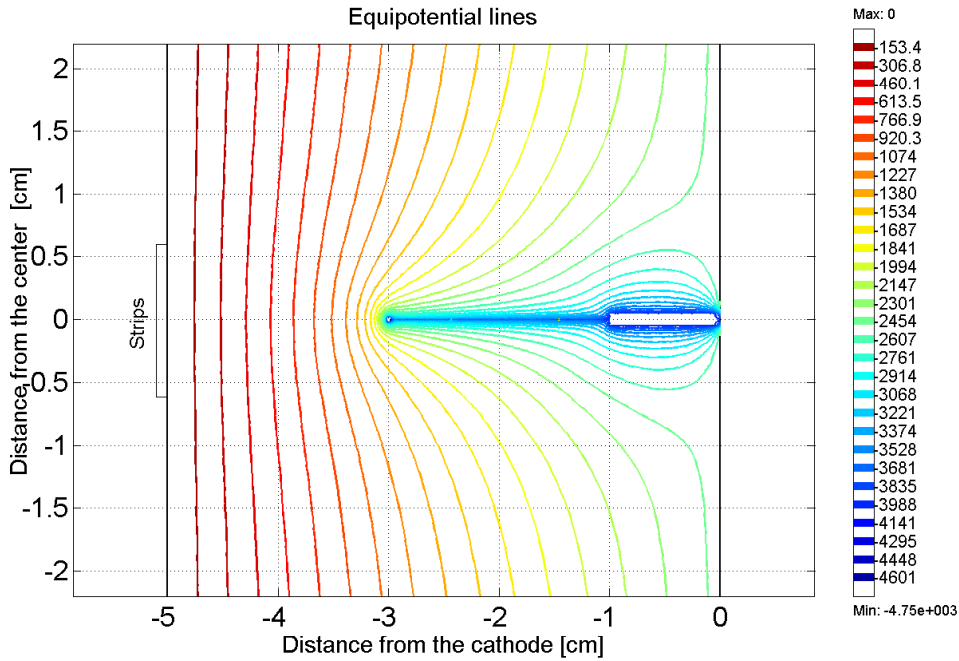


Figure 2.3: Equipotential lines in the drift chamber for -2,5kV on the cathode, -4kV on the source sphere and the anode with the strips on ground

The radioactive source covers the whole sphere and even a few millimeters of the support wire. Electrons from the α -particles emitted from the wire or from the half-sphere close to the wire can reach the outer strips, hence

we expect to detect the electrons on all strips.

The electric field, calculated on a line in the center of the drift chamber from the source sphere surface to the anode, is represented in Figure 2.5.

We notice that a very high field is expected close to the sphere surface.

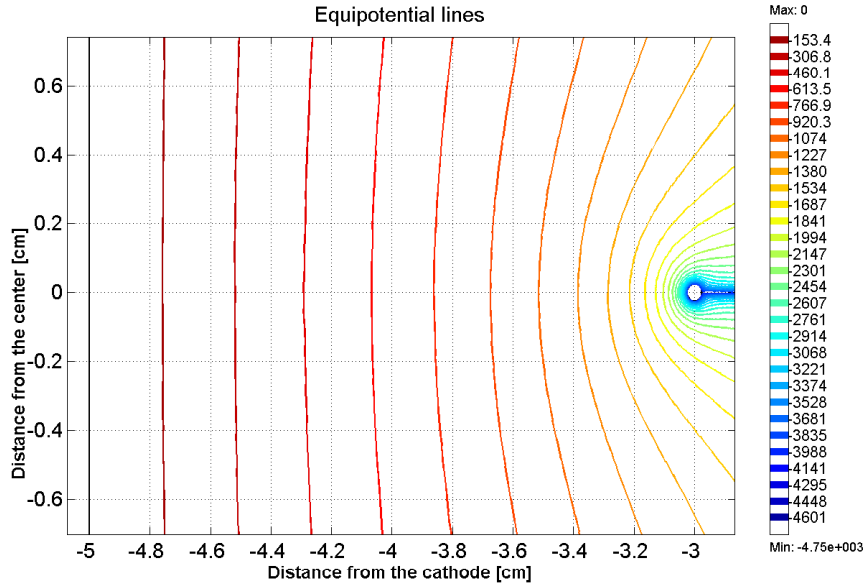


Figure 2.4: Equipotential lines in the drift chamber for -2,5kV on the cathode, -4kV on the source sphere and the anode with the strips on ground.

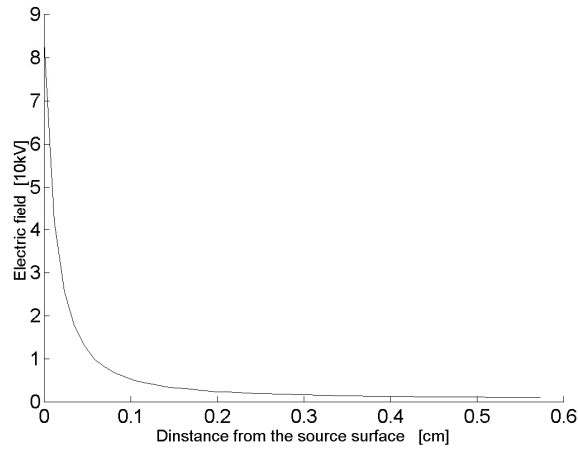


Figure 2.5: Electric field on the shortest distance between source and anode as a function of the distance.

Chapter 3

Experimental setup and measurements

3.1 Measuring setup and LAr filling procedure

Figure 3.1 shows the set-up used to test the drift chamber. Before filling the glass dewar with LAr, a good vacuum of the order of 10^{-6} mbar was reached using the turbo pump: the whole chamber and cables are inserted in the glass dewar; the vacuum chamber is heated and pumped for two days, so that most of the water contained in the set-up is evacuated. When a good vacuum is reached, before filling, the turbo pump is disconnected.

When filling, the argon flows from the argon dewar with an absolute pressure of about 2 atm through the filter, where it is cooled by liquid nitrogen, and goes then in the glass dewar. The outgoing valve is opened in order to reach a difference between the pressure of the ingoing argon and the pressure of the outgoing argon of about 0,4 atm. In about 3 hours the glass dewar is full with liquid argon.

3.2 Electronics

3.2.1 The high voltage

The high voltage is connected to the cathode and to the source through two coaxial teflon cables with an SHV connector. The high voltage cables are connected to the chamber through a 2,2nF capacitor and the source cable through a $50\text{M}\Omega$ resistor, too (see Figure 3.2).

3.2.2 The signal read-out chain

To read-out the 13 anode strips and the signal from the source, only 4 amplifier channels were available.

The source signal is used in a software trigger: when a signal is measured at

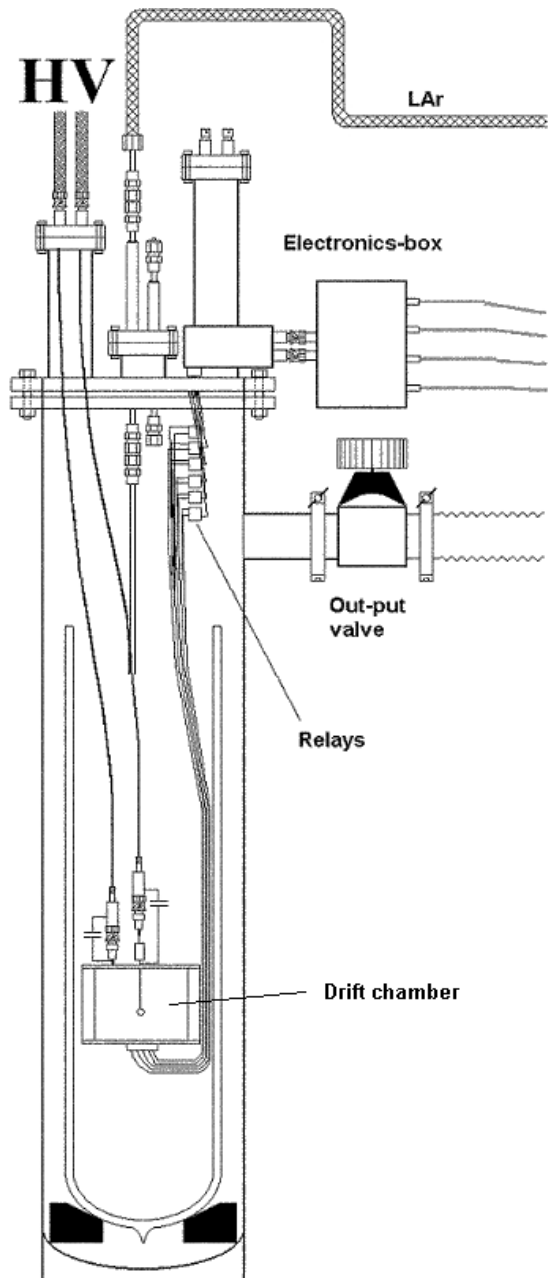


Figure 3.1: Schematic view of the measuring setup.

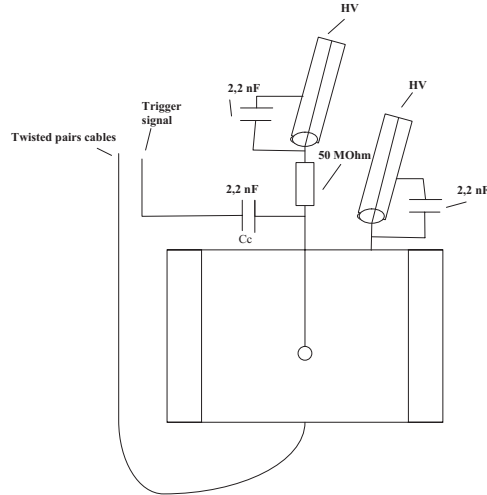


Figure 3.2: Connection of high voltage and trigger to the chamber.

the source, i.e. when an α - or β -particle is emitted, the signal is registered. One of the 13 twisted pair cables is used for that purpose. The trigger cable is connected to the source through the Cc, a 2,2nF coupling capacitor (see Figure 3.2).

The 13 strips on the anode are connected through an IDC connector to a twisted pair flat cable. Only 12 strips are measured because one of the 13 twisted pair cables is used for the source signal. The twisted pair cable conducts the signals to the relays (see Figure 3.3). From the relays the signal is then conducted to the outgoing vacuum feedthrough connector (Fischer connector) with 8 pins.

One of these pins has to be used for the trigger channel and one for the ground. We still have 12 strips and we need to measure them with the 6 remaining feedthrough pins. For this purpose we used 6 latching relays NAI S TQ2-L-5V.

Latching relays were used so that, once the relays are set correctly, the control-box can be disconnected from the feedthrough in order to avoid a lot of noise.

If we label the 12 strips from 1 to 12, then on the first pin, using a relay, we can measure strip 1 or strip 7, on the second strip 2 or strip 8 and so on (see Figure 3.3). In this way the signals of all 12 strips are available outside the vacuum chamber, six of them at the same time. The 8 outputs (6 strips, the trigger and the ground) are connected to 8 cables in a shielded box. The 8 cables can be connected to ground or through the 4 outputs to the electronic-board. For the control of the relays and the temperature measurement two additional Fischer connectors on the flange were used.

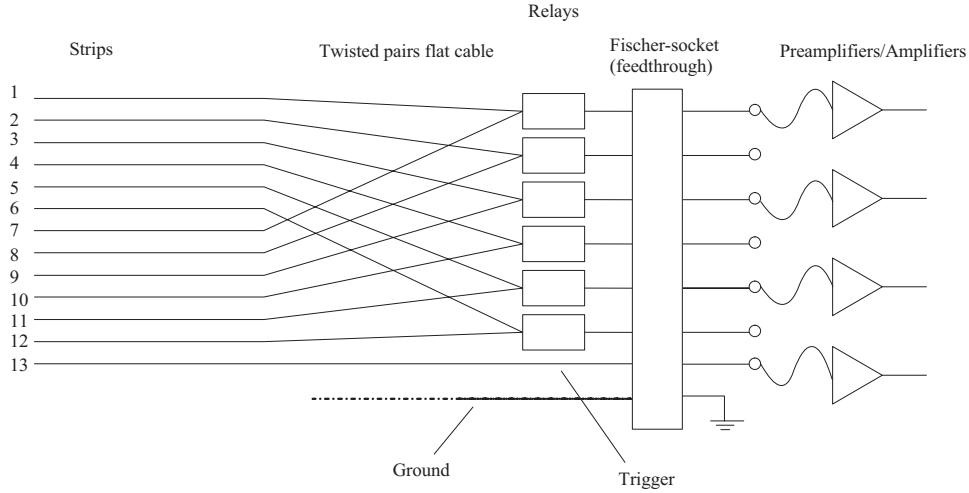


Figure 3.3: Schematic diagram of the read-out chain.

3.2.3 Electronic board

The electronics to measure the signals of the strips and of the source (trigger) is shown in Figure 3.4.

It operates at room temperature and has five input channels: one for the source, three for the strip signals (the PCI-card has only 4 input channels) and one for the calibration. For the source and strip channels the electronics is composed of a preamplifier, which acts as a charge to voltage converter, followed by two amplifier stages in cascade with a high-pass filter, which permit to adapt the output in the $\pm 1V$ range of the PCI card, and a baseline adjuster.

The voltage supply for the preamplifier is set at +12V and -5V.

The two amplifier stages have a gain of 10 each. The scheme of the output amplifier, with the high-pass filter, is sketched in Figure 3.5. The amplification is $A = \frac{R_2}{R_1}$. The C1 capacitor with the resistors R1 and R2 acts as a high-pass filter.

3.2.4 Calibration

Linearity of the read-out electronics

In order to test the linearity of the four channels and to determine the charge to voltage conversion factor (calibration), a rectangular signal is injected in the electronics.

The 5pF capacitor at the channel inputs (see Figure 3.4) has the following effect on a rectangular signal: the capacitor transmits a signal only when there is a potential slope dV/dt . With a rectangular signal as input, the

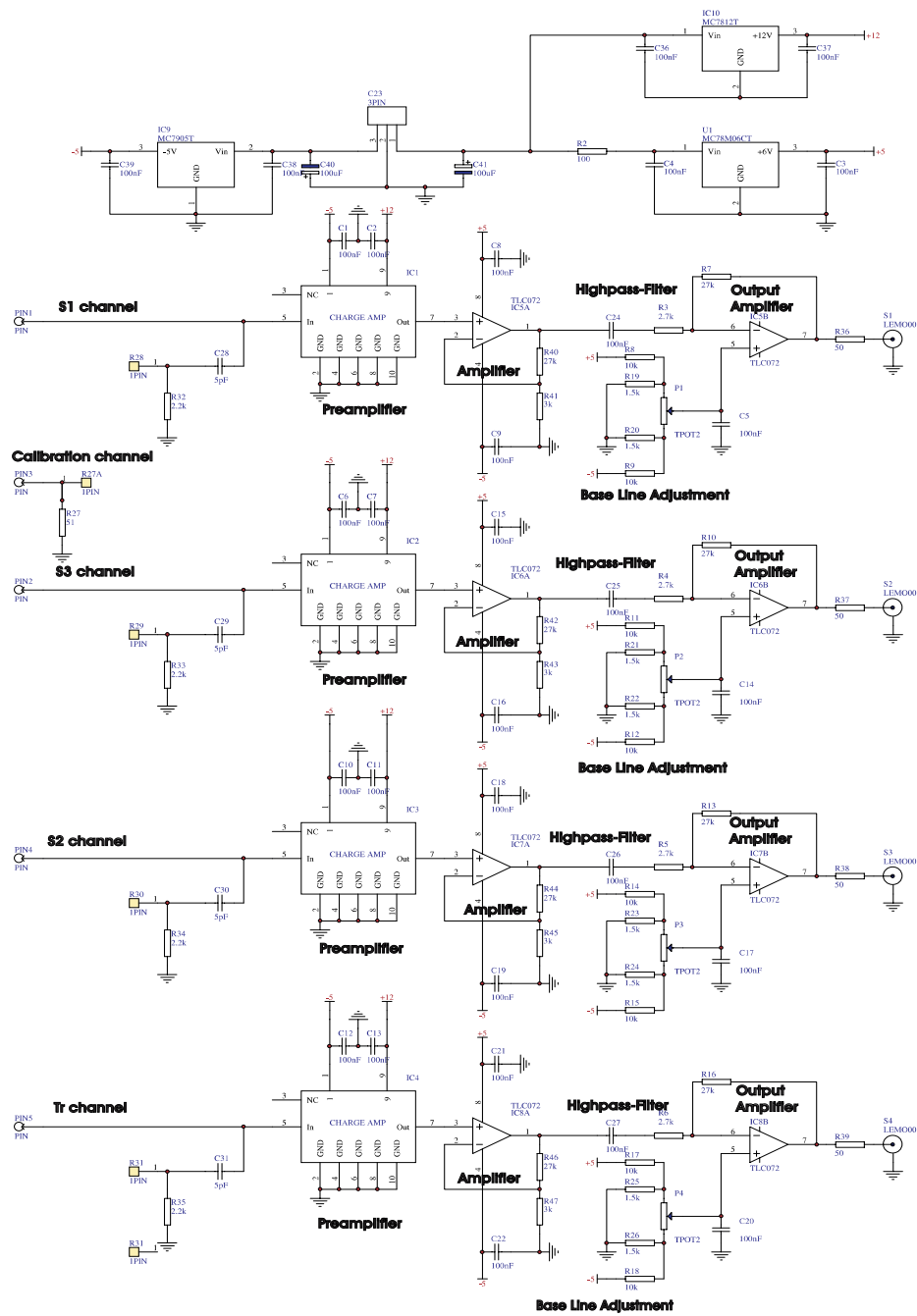


Figure 3.4: Scheme of the electronic-board.

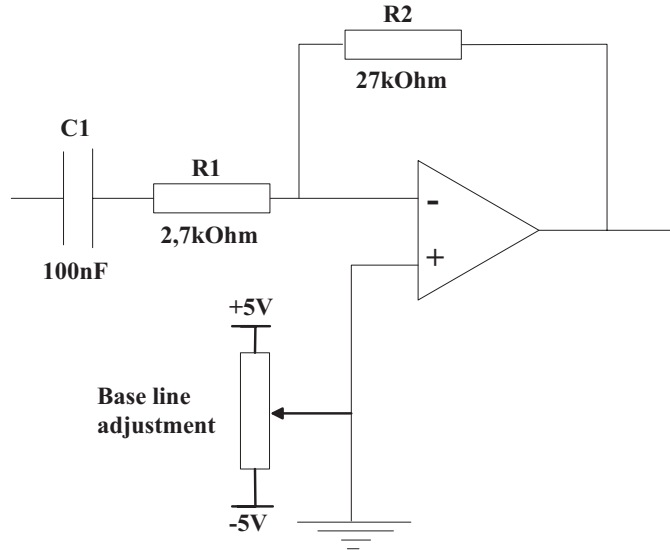


Figure 3.5: Scheme of the second amplifier stage with high-pass filter.

idealized output current signal is a δ -function.

The current is

$$I = C \cdot \frac{dV}{dt}. \quad (3.1)$$

If we integrate both sides, we get:

$$\int I \cdot dt = C \cdot \int \frac{dV}{dt} \cdot dt \quad (3.2)$$

Thus, we obtain the formula

$$Q = C \cdot \Delta V \quad (3.3)$$

Where ΔV is the peak to peak potential difference.

Three different rectangular signals were injected in the electronics: one with $\Delta V = 1V$, corresponding to $31,25 \cdot 10^3$ electrons, one with $\Delta V = 0,8V$, that is $25 \cdot 10^3$ electrons and one with $\Delta V = 0.64V$, that is $20 \cdot 10^3$ electrons. The frequency of the injected signals is in the three cases $\nu = 123,45678Hz$, a number that should not be a multiple of the power line frequency, 50Hz. For this three different pulses a sample of 5000 events has been taken with the data-acquisition Labview program and then analysed with the Fortran program as the signals (see Chapter 4). The analysis program calculates for each event the maximum of the pulse height. For each channel the pulse height spectrum is then plotted: we obtain a Gauss-distribution. This Gaussian has been fitted (see Figure 3.6) and the average of the pulse height has been calculated. The values of these averages are given in Table 3.1.

| Injected charge [$10^3 el.$] | Source [ADC counts] | S1 [ADC counts] | S2 [ADC counts] | S3 [ADC counts] |
|-----------------------------------|------------------------|--------------------|--------------------|--------------------|
| 31,25 | 672,6 | 683,9 | 698,7 | 658,0 |
| 25 | 547,5 | 553,4 | 569,3 | 534,1 |
| 20 | 437,0 | 445,6 | 458,8 | 429,8 |

Table 3.1: Average over 5000 events of the pulse height measured by injecting in the electronic a rectangular signal.

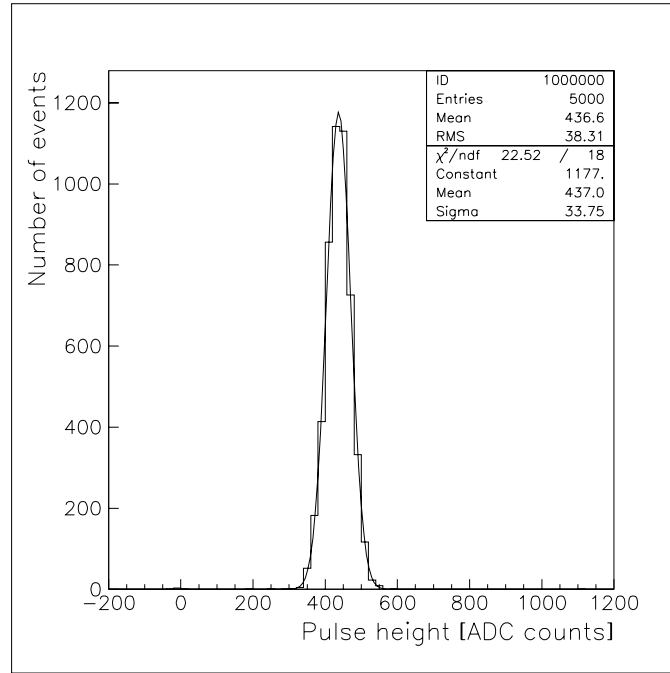


Figure 3.6: Pulse height spectrum of the trigger channel for a square signal corresponding to $20 \cdot 10^3$ electrons.

Figure 3.7 shows the mean pulse height as a function of the injected charge. The point at 0 has been added to the plots. The slope of the four lines is written on the graphic statistics with the name P2. The slope was calculated by linear fitting the points of the graphics. In fact, the slope has been calculated in two ways, first by considering only the three measured points and then by considering the points at 0 as well. The results are summarize in Table 3.2. For the following conversion from ADC counts to the charge in number of electrons, the slope obtained by considering the point (0,0) is used.

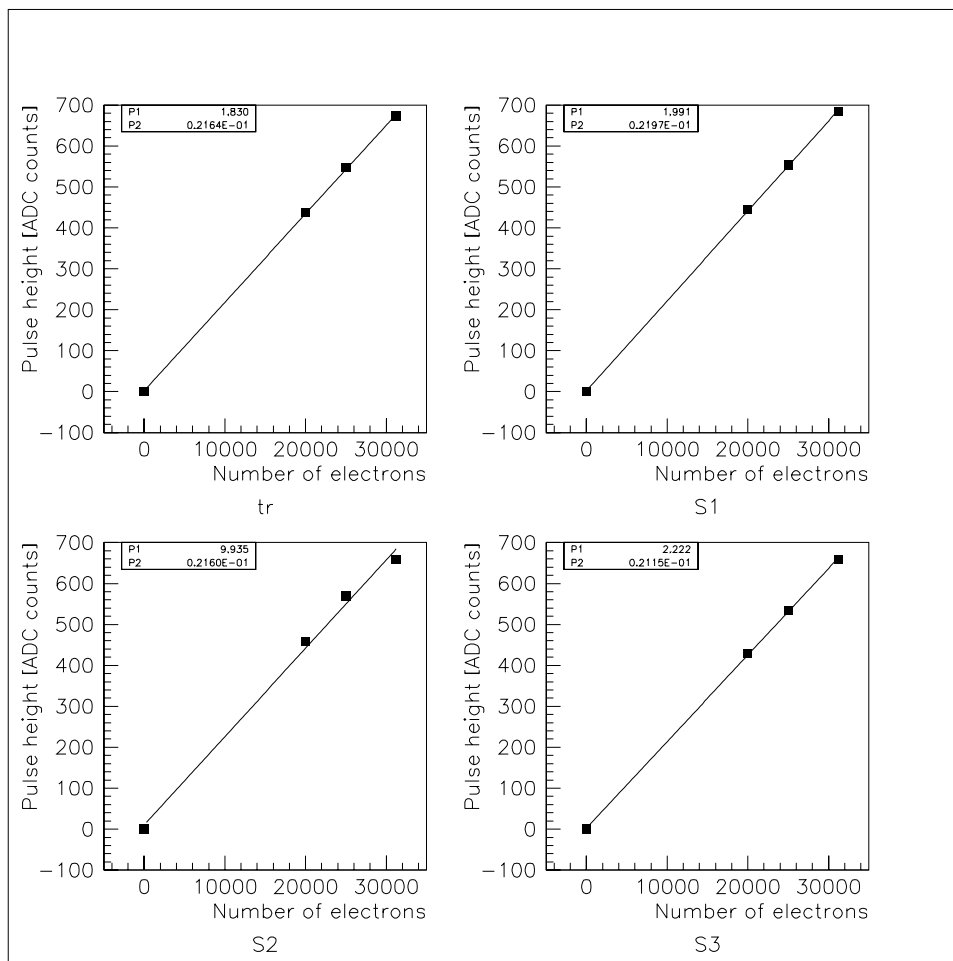


Figure 3.7: Linearity of the four read-out chains.

| | Slope of tr channel [$\frac{ADC}{10^3 el.}$] | Slope of S1 channel [$\frac{ADC}{10^3 el.}$] | Slope of S2 channel [$\frac{ADC}{10^3 el.}$] | Slope of S3 channel [$\frac{ADC}{10^3 el.}$] |
|---------------------|--|--|--|--|
| without point (0,0) | 20,90 | 21,17 | 17,63 | 20,27 |
| with point (0,0) | 21,64 | 21,97 | 21,60 | 21,15 |

Table 3.2: Slopes of linearity test measurements.

Cross-talk

The cross-talk between the strips has also been tested, with strips 4 soldered to the S1 channel, strip 9 to the S3 channel and strips 5,6,7,8 soldered to the central channel. First, the channel S2 is disconnected from the calibration pulse input (but still connected to the strips) and in channels S1, S3 and Tr a large rectangular signal of $\Delta V = 6V$ (corresponding to $187,5 \cdot 10^3$ electrons, saturating the ADC) is injected. In this way the cross-talk between S2 and the other channels is checked. Then channels S1 and S3 are disconnected from the calibration input and in S2 and Tr a rectangular signal of $\Delta V = 10V$ (corresponding to $312,5 \cdot 10^3$ electrons) is injected.

Figure 3.8 shows the pulse height histograms for the cross-talk of channel S2 with channels S1 and S3 (hatched histograms) and for the noise (white histograms): we see that the pulse height distribution for the S2 channel is very similar to the noise histogram.

Figure 3.9 shows the cross-talk of channels S1 and S3 with channel S2. Here, too, we see that the cross-talk between channels is negligible.

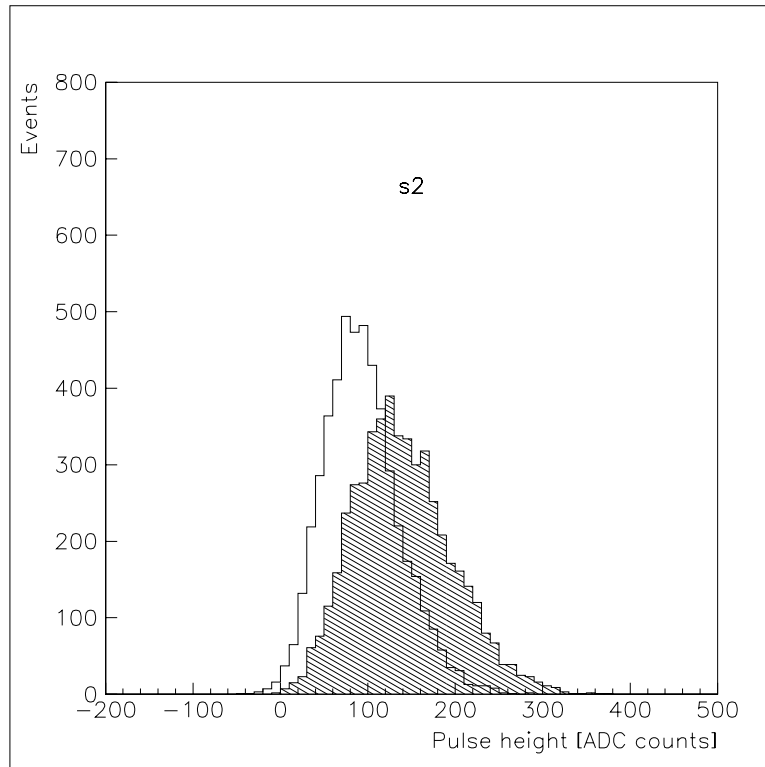


Figure 3.8: Cross-talk: signal injected on S1 and S3 and tr channels; hatched histogram: channel S2, white histogram: noise.

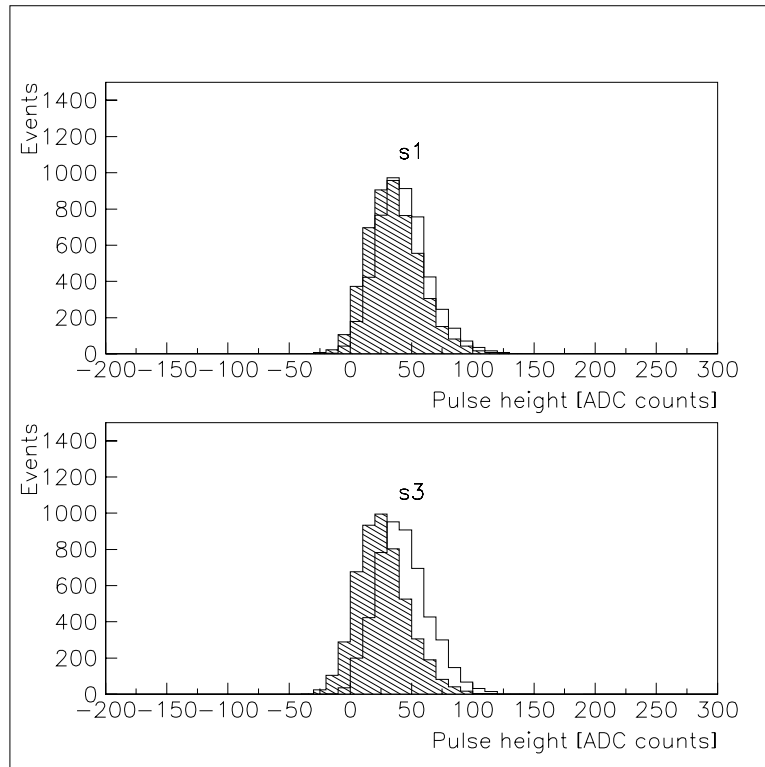


Figure 3.9: Cross-talk: signal injected on S2 and tr channels; hatched histograms: channels S1 and S3, white histograms: noise.

Chapter 4

Data acquisition and analysis

4.1 Data acquisition

The data are collected with an ADC PCI card (see description in Table 4.1) [8] and pre-analysed with a Labview data-acquisition program called DAQ 17-06-2002.vi.

| | |
|------------------------|---|
| Card type | PCI-DAS4020/12 |
| Resolution | 12 bits |
| Number of channels | 4 single ended, 1 A/D per channel |
| Coupling | DC |
| A/D conversion time | 40 ns |
| Input bandwidth | 17 MHz |
| Maximum sampling rates | 1 and 2 channels 20 MHz; 4 channels 20 MHz |
| Minimum sampling rate | 1kHz |
| Input Impedance | 50 Ω or 1.5M Ω |
| Input range | $\pm 1V$ or $\pm 5V$ |
| Trigger modes | A/D and/or gate Pre and post trigger |

Table 4.1: Main characteristics of the PCI card.

The PCI card has only 4 channels. One channel is used for the source and the other 3 channels are left for the strips. We used a sampling rate of 10 MHz for each of the four channels.

The data, collected from the four channels were filled through the 'Foreground Analog input Scan' in a vector with the size of the parameter Count (1'000'000 in our case).

No hardware trigger was used for the data acquisition, the signal was continuously recorded. In the data-acquisition program a software trigger, based on the source signals, was used. The software trigger is here described.

The points from the source signal (channel 4) are separated from the others, so that the signals of the source may be searched. In order to eliminate the noise, the source signal is filtered using the moving average method with a 100 samples period (an average over the first 100 samples is calculated and then subtracted from the first point, then an average from point 2 to point 101 is calculated and subtracted from the second point, and so on).

Then, a numerical differentiation of the source signal is done: the first point of the signal is subtracted from the hundredth point (so that, if one of these points belongs to the signal step, the other one surely not), then the second point is subtracted from the hundred-and-first point, and so on. In this way the signal is transformed into a very well localized, sharp peak (see Figure 4.1).

After that, all the peaks in the $1'000'000/4=250'000$ points of the source data are detected with the 'peak detector' *.vi program (in Labview): only peaks, that (after filtering and differentiating) are bigger than 300 ADC counts are stored for the further analysis.

Figure 4.1 shows an example of the different steps for this peak search of the source channel: the first plot represents a typical raw signal of the source; the second plot represents the source signal after having been filtered; the third plot represents the source signal after having been filtered and numerical differentiated; also the threshold at 300 is drawn in the third plot.

For every peak found, except for those which occur at times bigger than $(\text{Count}/4)-10'000$, an event matrix containing $10'000$ raw data points with 2000 points before the source peak maximum, containing the four channels, is created. The raw signals from the strips and the source for a typical event are shown in Figure 4.2. We notice the trigger signal and a signal in channels S2 and S3. We approximately calculated from the observed signal a drift time of the electrons from the source to the strips of about $13 \mu\text{s}$.

With this data acquisition program we observed during the measurements two different kinds of bad source events: the first type with big and fast oscillations of the source signals, probably coming from some problem with the high-voltage; the second type, which occurred at a rate that increased with time, saturated the ADC, as shown in Figure 4.3. This second kind of bad events may come from bubbles in the LAr; in fact the number of this kind of bad events has increased with the time, when the temperature of the argon increased and the argon boiled.

The pulse height distribution of the trigger signals, after having been analysed with the analysis program (see Section 4.2) is plotted in Figure 4.4. We observe three peaks: the first represents small signals, that is β -particles or noise; the second represents the α -particles; whereas the third represents bad events.

From this histogram we notice that the choice of taking into account only signals with a filtered and differentiated source signal bigger than 300 ADC counts is a good choice: in fact, with this threshold we still collect β -particles

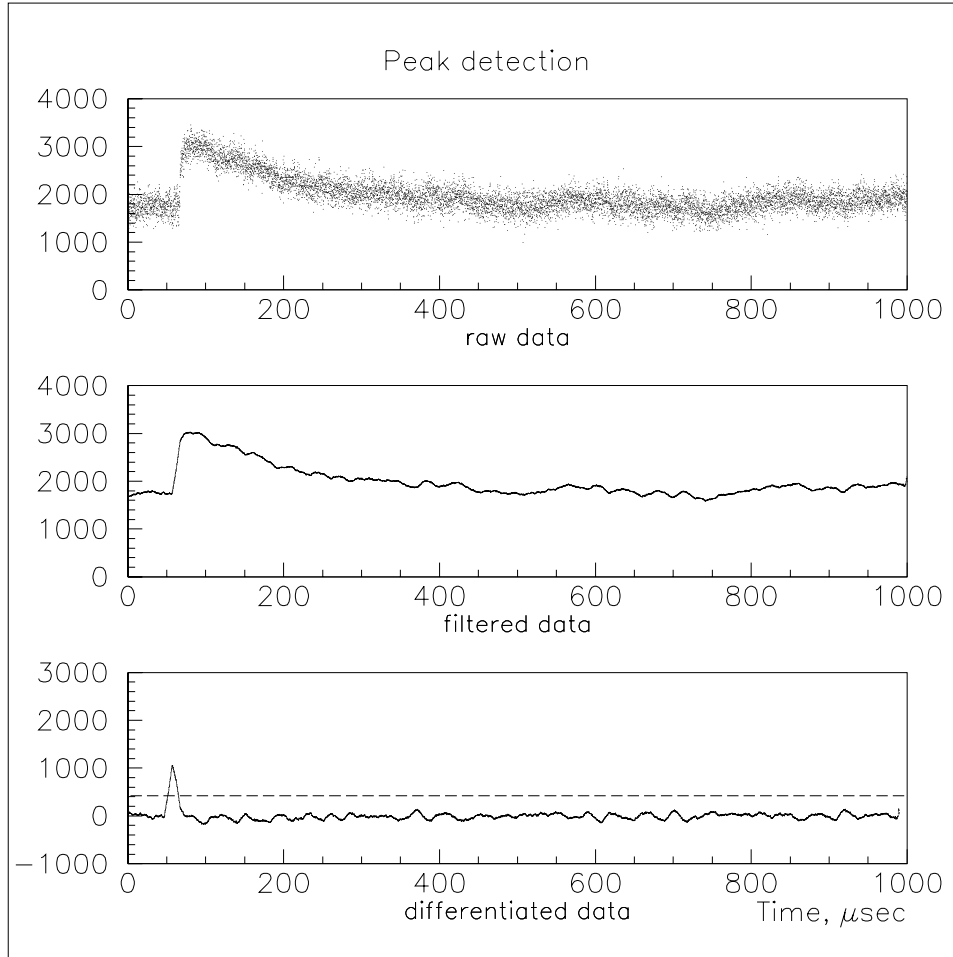


Figure 4.1: The three steps of the signal search in the source data (trigger): 1.The source raw data, 2.The filtered source data, 3.The filtered and numerical differentiated source data. The threshold at 300 ADC counts is also shown.

and noise and we collect all the α -particles; in this way we can clearly see where the peak of the α -particle begins.

In order to eliminate the bad events, the rate of which increased with time, a further filter has been inserted in the data acquisition program: if the maximum of the trigger raw data is equal to 4095 counts (saturation of the ADC) or the minimum is equal 0, the signal is not recorded.

This additional filter was inserted between the measurements with one strip in the central channel and the measurements with two strips in the central channel (see Chapter 5). With this filter we eliminate almost all the bad events.

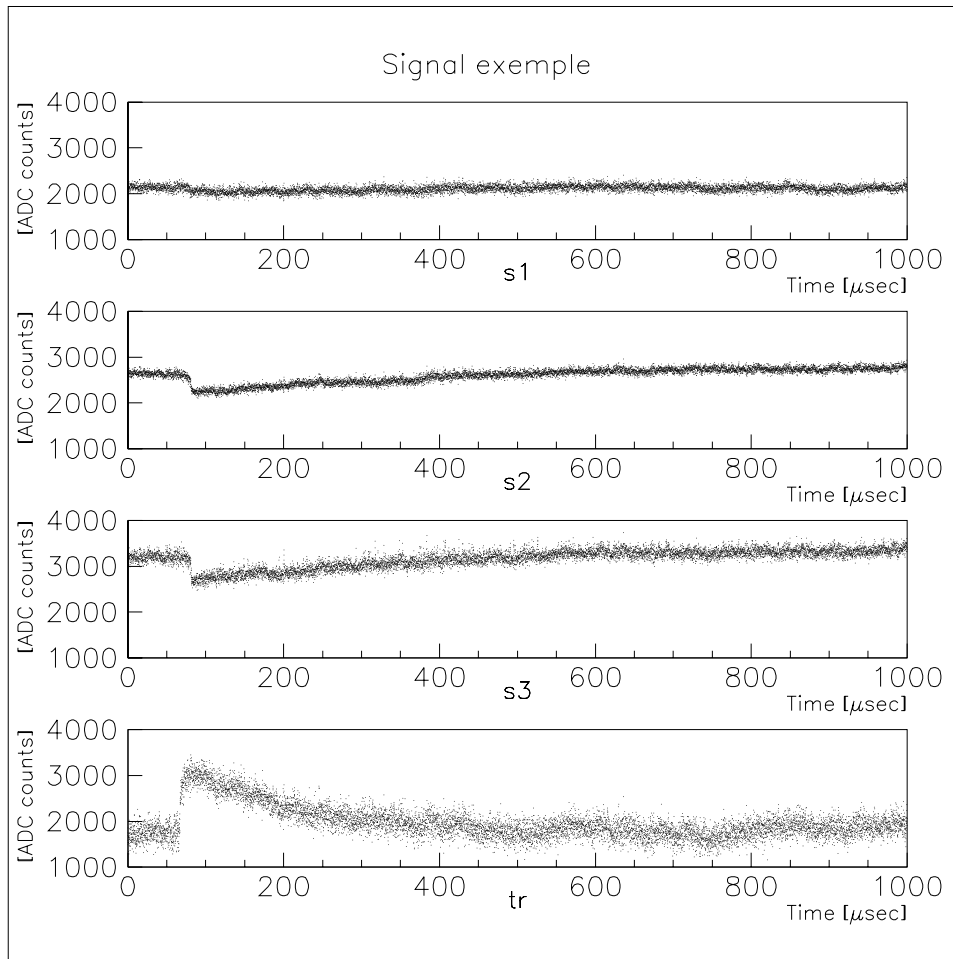


Figure 4.2: Example of an observed event (raw-data)

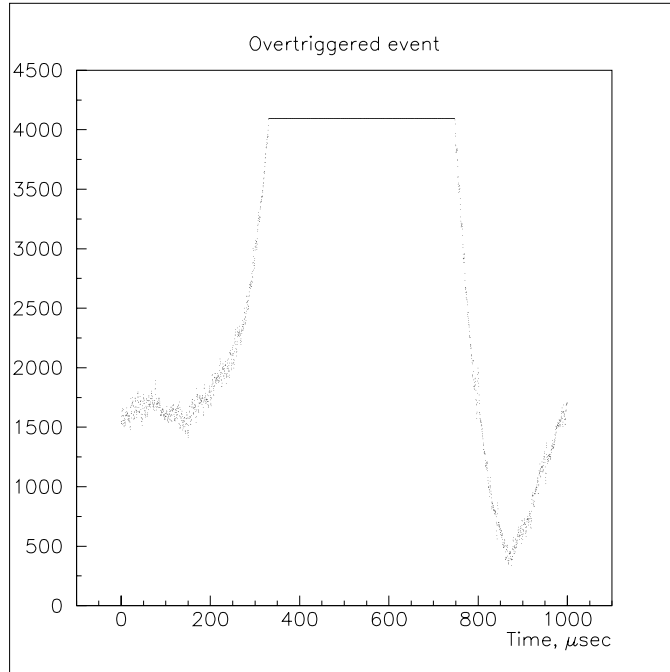


Figure 4.3: Example of a bad event saturating the ADC.

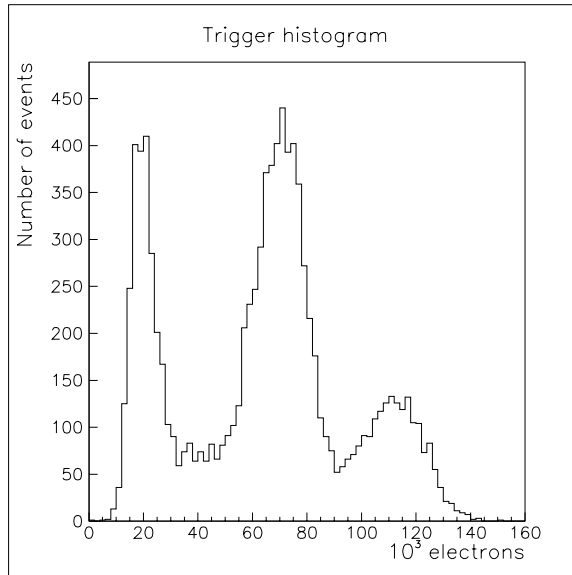


Figure 4.4: Pulse height distribution of the trigger signals.

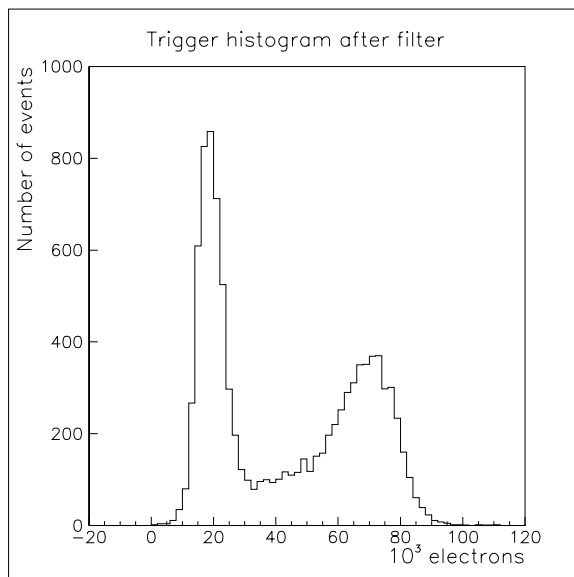


Figure 4.5: Pulse height distribution of the trigger signals with cuts after the saturation filter.

Figure 4.5 shows the histogram of the analysed trigger channel after this filter has been applied.

We observe that the third peak, corresponding to bad signals, disappears. With this data acquisition program I recorded from 5000 to 10000 (when the saturation cut was not included) events for each measuring condition (see Section 5.1).

The data are saved in a *.bin format.

4.2 Data analysis

The data recorded by the Labview program have to be converted in order to be read with a Fortran program. The *.bin file from the data acquisition is converted to a *.binF file, which can be read by Fortran.

The collected data are then analysed with a Fortran program, which calculates the charge corresponding to a signal for each channel in the following way:

- The recorded vector containing the raw data is split in the 4 different channels.
- Each channel is filtered twice in order to suppress the noise:
 - Filter 1: the most frequent value occurring over the first 500 points is calculated; this value is then subtracted from the first point. Then

the most frequent value occurring between point 2 and point 501 is calculated and is subtracted from the second point, and so on for the whole channel window.

Filter 2: a moving average with 100 samples period is applied.

- For each event filtered twice the pulse height maxima of the four channels is calculated and recorded in a *.txt file.

A typical trigger event, that has been filtered with the two filters, is shown in Figure 4.6.

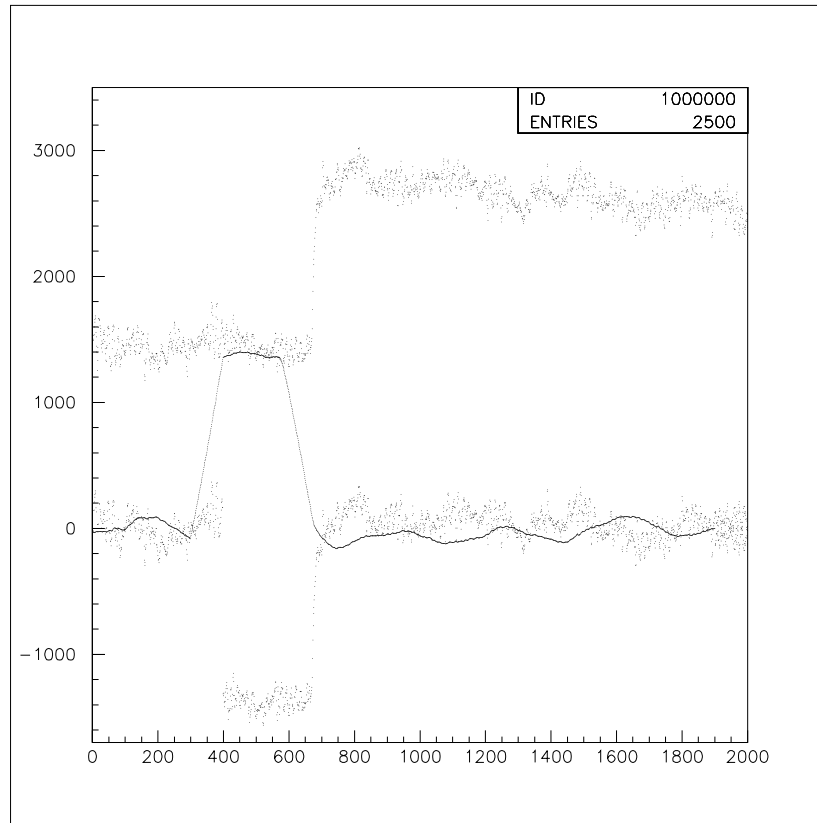


Figure 4.6: Raw-data of the source (top), filtered with filter 1 (bottom), and filtered with both filters (and inverted, middle).

The pulse height (plateau) of the double filtered signal is a measure for the charge corresponding to this signal. The maximum value of the plateau is used to calculate the charge. The factor to convert ADC counts into a charge is obtained from the calibration measurements (see Table 3.2).

Chapter 5

Results

5.1 Measurement program

An α -particle ionizes the LAr in a range of $50 \mu\text{m}$ [9]; if the α -particle is emitted in the field line direction, all the electrons should have more or less the same trajectory and the event should be well localized on the anode. The diffusion of the electron cloud in the drift space is given from the equation:

$$\sigma_D = \sqrt{2 \cdot D \cdot t_{drift}} \quad (5.1)$$

Where D is the diffusion coefficient of LAr and measures $D = 5\text{cm}^2/\text{s}$.

For the drift time t_{drift} we used the value of $13 \mu\text{s}$. Thus, we reach for the diffusion of the electrons a value of $\sigma_D = 0.11\text{mm}$, that means that 95% of the electrons at the end of the drift space are localised on a cloud with $4 \cdot \sigma_D = 0.44\text{mm}$ of diameter.

From this result we can say that the most part of the events coming from an α -particle emitted in the field line direction are detected from only one strip. Some cases of these events detected on two adjacent strips can however occur.

If the emission of the α -particle is not along a field line, then the event will be recorded on more strips.

In fact there are three angles which characterize the α -emission: we call them β , γ and δ and they are sketched in Figure 5.1. If the angle β is zero, then the α -particle is emitted in the direction of the field lines.

If it were possible to read the signal in two dimensions, with two wire layers perpendicular to each other, we could measure exactly the track of the electrons and we could calculate where and in which direction the α -particle was emitted.

In order to study the distribution of the different event types over the anode strips, measurements over all 12 strips have been taken. We observed events detected only by one strip, events detected by two adjacent strips, by three adjacent strips, by four adjacent strips and events not detected by any strip.

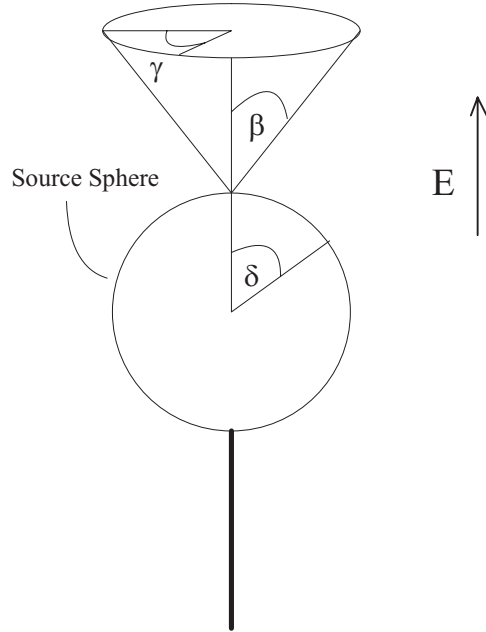


Figure 5.1: Definition of the angles β , γ and δ which characterize the α -emission.

For each strip combination measured we also measured the two neighbouring strips at the edge and used them as veto: in this way, with the appropriate cuts, it is possible to define how many events are detected by the central channel but not by the two veto channel. We first measured all the strips individually with the two neighbouring strips as veto, then all the possibilities for two adjacent strips soldered together in the central channel and two neighbouring strips as veto, then for three strips and at the end for four strips soldered in the central channel.

For one strip in the central channel we recorded 10'000 events; for two strips soldered in the central channel we recorded 10'000 events with the saturation filter on the source signal included (see Chapter 4); for three and four strips soldered in the central channel we recorded only 5000 events with the saturation filter included, because almost all the bad source events were eliminated. The measurements were taken from the 8 to the 11 July 2002.

5.2 Results of the measurements with 12 strips

5.2.1 The cuts

First of all a cut on the trigger signal as shown in Figure 5.2 and Figure 5.3 is applied. Only trigger signals smaller than $87.5 \cdot 10^3$ electrons and bigger

than $50.6 \cdot 10^3$ electrons are taken into account, that is only signals corresponding to α -particles. The first peak in Figure 5.2 corresponds to the noise or the β -particles, whereas the third peak corresponds to bad events, which could be bubbles in LAr passing by the source. In Figure 5.3 the peak corresponding to bad events has disappeared after the saturation filter (see Chapter 4) has been applied.

In order to know how many events are measured in the central channel but not in the two veto strips, cuts on the three signal channels are applied: First, as shown in Figure 5.4, only signals bigger than $9 \cdot 10^3$ electrons in the central channel and smaller than $6, 9 \cdot 10^3$ electrons in the veto channels are taken into account. The big peak in the histograms for S1, S2 and S3 in Figure 5.4 is given by noise.

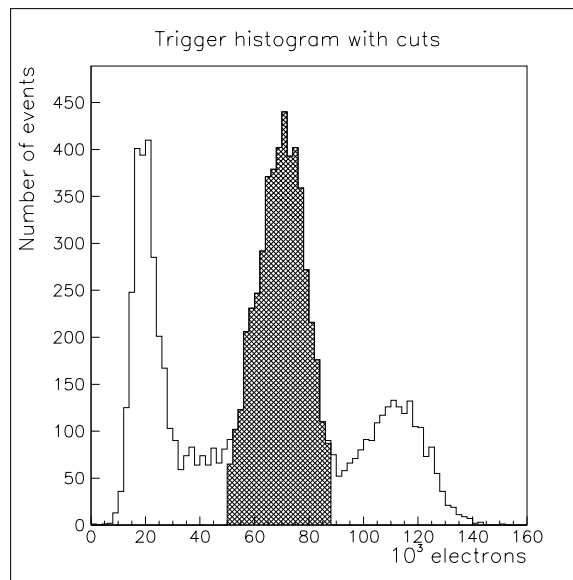


Figure 5.2: Pulse height distribution of the trigger signals. The cuts selects the events in the cross-hatched area.

After these cuts have been applied, the plots of the remaining events have been studied. The four scatter plots of the remaining events for 1, 2, 3 or 4 strips in the central channel are shown in Figure 5.5. In this figure the pulse height of the central channel S2 versus the sum of the pulse height of the two veto channels S1 and S2 is plotted. In the four cases we notice two groups of events: events that have a big pulse height in the central channel, about $60 \cdot 10^3$ electrons, that is of the same order as the source pulse height; and events with a smaller pulse height in the central channel, about $10 - 20 \cdot 10^3$ electrons, which are clearly noise events.

A further cut is applied to the central channel S2: only signals bigger than $30 \cdot 10^3$ electrons are taken into account.

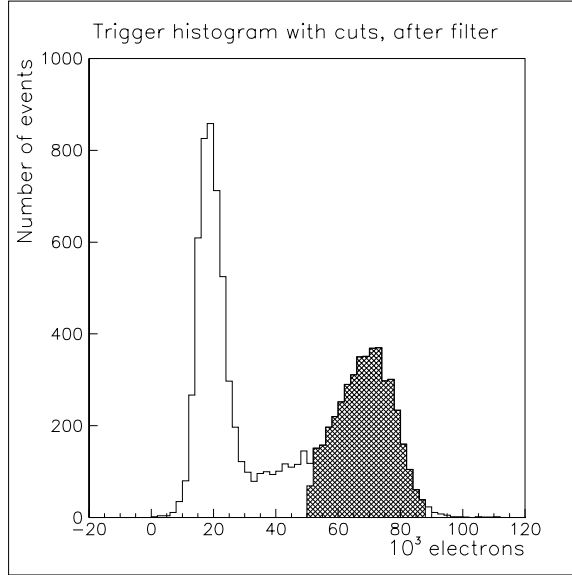


Figure 5.3: Pulse height distribution of the source with cuts after the saturation filter.

By applying all these cuts together we find the number of events with a good trigger, which are registered in the central channel but not in the veto channels. Since the data acquisition program was modified during the measurements and the number of good source events is not constant during the measurements, we calculate the fraction of the events for each strip combination, obtained by dividing the number of events with the number of good trigger events.

5.2.2 The results

For every strip and every group of strips we collected the number of events remaining after the cuts were applied.

The results of these measurements are summarized in Table 5.1 and presented in Figures 5.6, 5.7, 5.8, 5.9. Note, that the data of neighbouring bins in Figures 5.7, 5.8 and 5.9 contain common strips, i.e. they are not independent from each other.

The 'Number of events' given in Table 5.1 is the total number of events detected from the given strips: for example the 103 events measured on strips 2 and 3 are the sum of the events detected only by strip 2, the events detected only by strip 3 and the events detected by both strips.

In the 'Percentage of events' in Table 5.1 and in the four Figures 5.6, 5.7, 5.8, 5.9, on the contrary, only the events detected exactly by 1, 2, 3 or 4

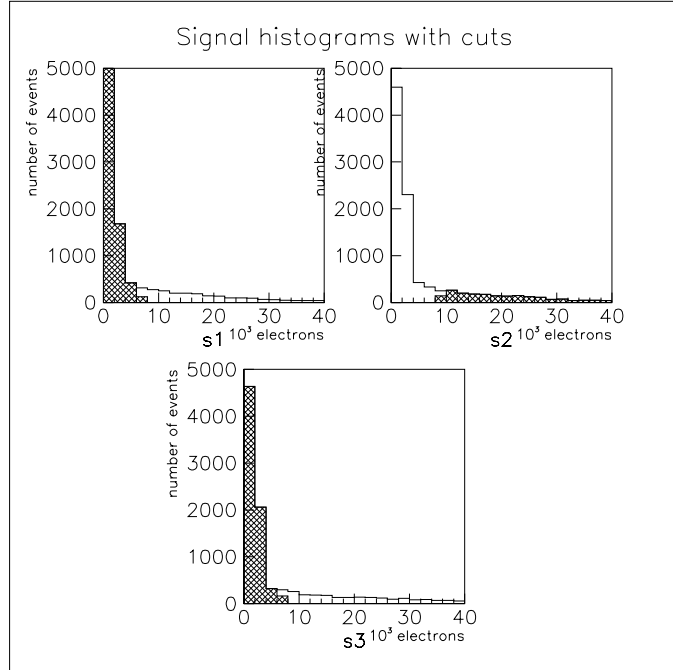


Figure 5.4: Pulse height distribution of the three strip signals for the strip 2 soldered to the central channel S2 and strips 1 and 3 as veto in S1 and S2.

strips respectively, are taken into account. For example from the percentage of events detected by strips 2 and 3 the percentage of events detected only by strip 2 and by strip 3 are subtracted.

5.2.3 Discussion of the results

The results are summarized in the four Figures 5.6, 5.7, 5.8 and 5.9.

In Figure 5.6 the events detected by one strip in the central channel with the respective errors are shown, whereas in Figure 5.7 the events detected by two soldered strips with the respective errors are shown. In these two cases, particularly in Figure 5.6, we notice a certain structure in the event distribution. In Figure 5.6 we observe a clear maximum in the percentage of events on strip 4 and perhaps a minimum on strip 9. This event distribution is not symmetric with respect to the center of the chamber as we expected. The asymmetry may come from the fact that the source might not be exactly centered. In Figure 5.7 the maximum in the event distribution is much smaller and is shifted around strips 5 and 6; the minimum is around strips 7, 8 and 9 and another maximum appears around strips 10 and 11.

In Figure 5.8 and Figure 5.9 the events detected by three and four strips with the respective errors are shown. In these two cases we do not notice a

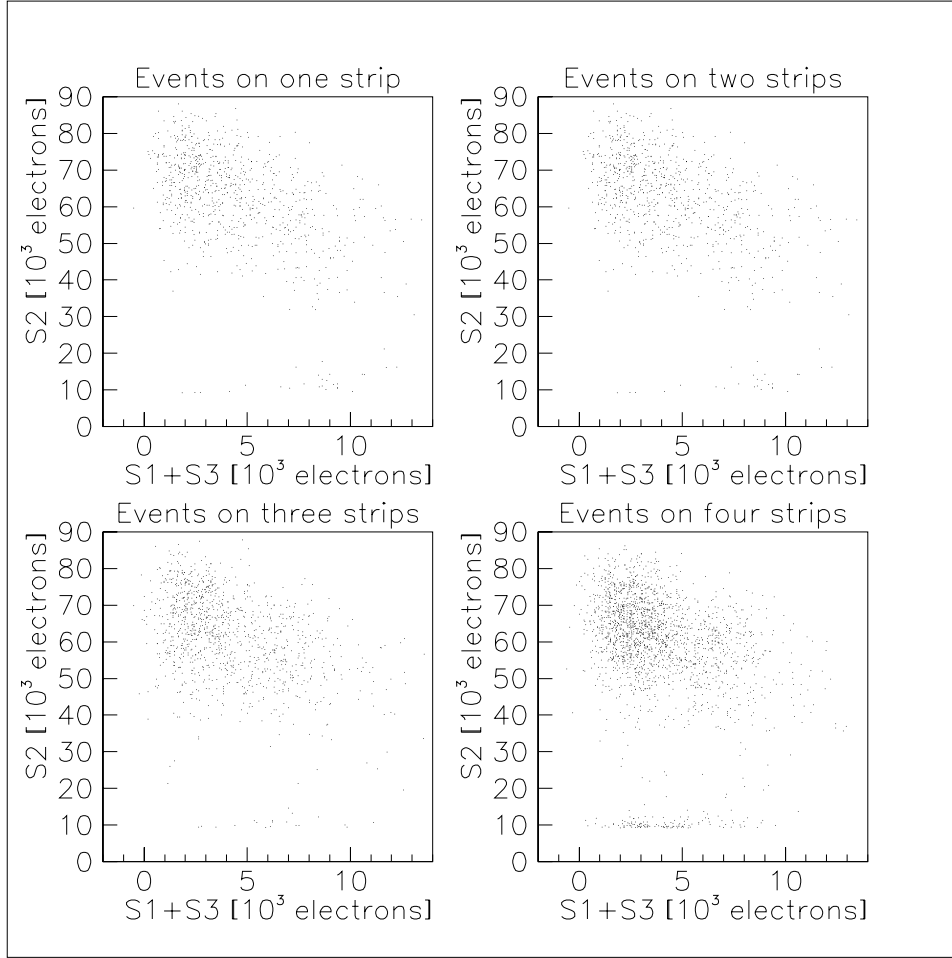


Figure 5.5: Events remaining after a lower cut of $9 \cdot 10^3$ electrons on the central channel and an upper cut of $6,9 \cdot 10^3$ on both the veto channels were applied.

particular distribution of the events on the strips, which are almost homogeneously distributed.

In the results for four strips soldered in the central channel we obtain some negative results. These negative results come from the subtractions performed to obtain the number of events detected exactly on 4 strips, and they don't have any physical meaning.

We may notice that the structure of the event distribution decrease as the number of strips soldered in the central channel increase.

The flat distribution observed in Figure 5.8 and Figure 5.9 might come from events which belong to the background, that is from some possible noise coming from the tail of the first peak in Figure 5.3. In order to know more

about that, the event distribution of the background has been studied as well. First of all the cuts on the trigger channel as shown in Figure 5.3 are inverted: we took the events with a trigger signal smaller than $50.6 \cdot 10^3$ electrons and bigger than $87.5 \cdot 10^3$ electrons, that is signals not corresponding to α -particles. Then this signals are analyzed exactly in the same way as the α -particle signals.

This background event distribution is shown in Figure 5.10. In all the four cases the percentage of events on each strip is much smaller than those of the event distributions of the α -particle. For that reason we can say that the background events are not the main responsible for the flat event distribution of Figures 5.8 and 5.9.

It is hard to guess the reason of the different distributions on the strips. In order to know more about that, an accurate simulation of the events has to be done and more measurements, perhaps with a board with more input channels, have to be taken.

| Strips measured | Strips used as veto | Number of events | Number of good trigger events | Percentage of events |
|-----------------|---------------------|------------------|-------------------------------|----------------------|
| 2 | 1 and 3 | 6 | 4873 | 0.123±0.050 |
| 3 | 2 and 4 | 17 | 5439 | 0.313±0.076 |
| 4 | 3 and 5 | 21 | 5167 | 0.406±0.089 |
| 5 | 4 and 6 | 12 | 4479 | 0.268±0.077 |
| 6 | 5 and 7 | 13 | 5438 | 0.239±0.066 |
| 7 | 6 and 8 | 7 | 4088 | 0.171±0.065 |
| 8 | 7 and 9 | 9 | 4939 | 0.182±0.061 |
| 9 | 8 and 10 | 3 | 4294 | 0.070±0.040 |
| 10 | 9 and 11 | 5 | 3689 | 0.136±0.061 |
| 11 | 10 and 12 | 7 | 3375 | 0.207±0.078 |
| 2 and 3 | 1 and 4 | 103 | 4641 | 1.784±0.234 |
| 3 and 4 | 2 and 5 | 90 | 4264 | 1.392±0.249 |
| 4 and 5 | 3 and 6 | 106 | 4285 | 1.799±0.265 |
| 5 and 6 | 4 and 7 | 107 | 4145 | 2.074±0.266 |
| 6 and 7 | 5 and 8 | 84 | 4235 | 1.573±0.233 |
| 7 and 8 | 6 and 9 | 49 | 3589 | 1.012±0.213 |
| 8 and 9 | 7 and 10 | 59 | 4292 | 1.123±0.192 |
| 9 and 10 | 8 and 11 | 87 | 4450 | 1.750±0.220 |
| 10 and 11 | 9 and 12 | 129 | 4381 | 2.602±0.274 |
| 2, 3 and 4 | 1 and 5 | 123 | 2111 | 1.809±0.627 |
| 3, 4 and 5 | 2 and 6 | 148 | 2288 | 2.321±0.645 |
| 4, 5 and 6 | 3 and 7 | 148 | 2260 | 1.761±0.655 |
| 5, 6 and 7 | 4 and 8 | 142 | 2303 | 1.840±0.625 |
| 6, 7 and 8 | 5 and 9 | 125 | 2272 | 2.325±0.583 |
| 7, 8 and 9 | 6 and 10 | 108 | 2332 | 2.074±0.530 |
| 8, 9 and 10 | 7 and 11 | 133 | 2357 | 2.383±0.566 |
| 9, 10 and 11 | 8 and 12 | 153 | 2279 | 1.949±0.640 |
| 2, 3, 4 and 5 | 1 and 6 | 229 | 2303 | -0.003±1.186 |
| 3, 4, 5 and 6 | 2 and 7 | 328 | 2811 | 1.095±1.200 |
| 4, 5, 6 and 7 | 3 and 8 | 274 | 2352 | 1.517±1.215 |
| 5, 6, 7 and 8 | 4 and 9 | 229 | 2391 | -0.106±1.132 |
| 6, 7, 8 and 9 | 5 and 10 | 218 | 2436 | 0.181±1.051 |
| 7, 8, 9 and 10 | 6 and 11 | 247 | 2506 | 0.957±1.048 |
| 8, 9, 10 and 11 | 7 and 12 | 308 | 2568 | 1.593±1.147 |

Table 5.1: Events measured only in the central channel.

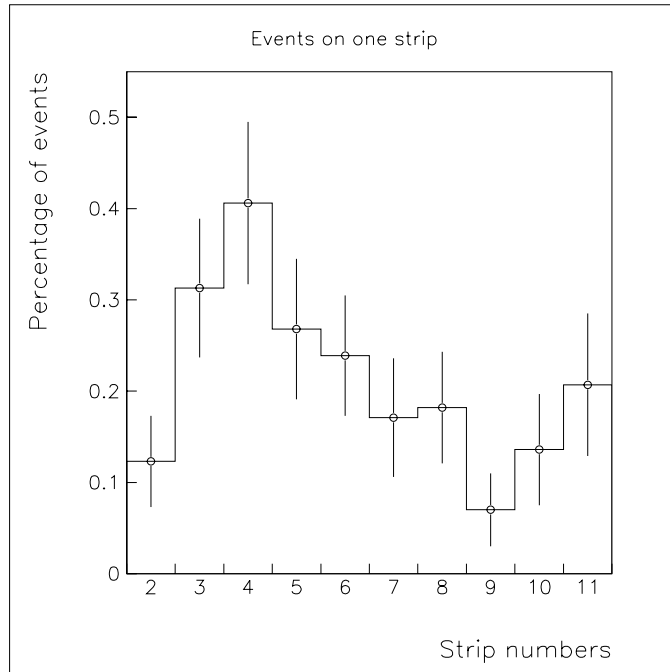


Figure 5.6: Events detected with only one strip.

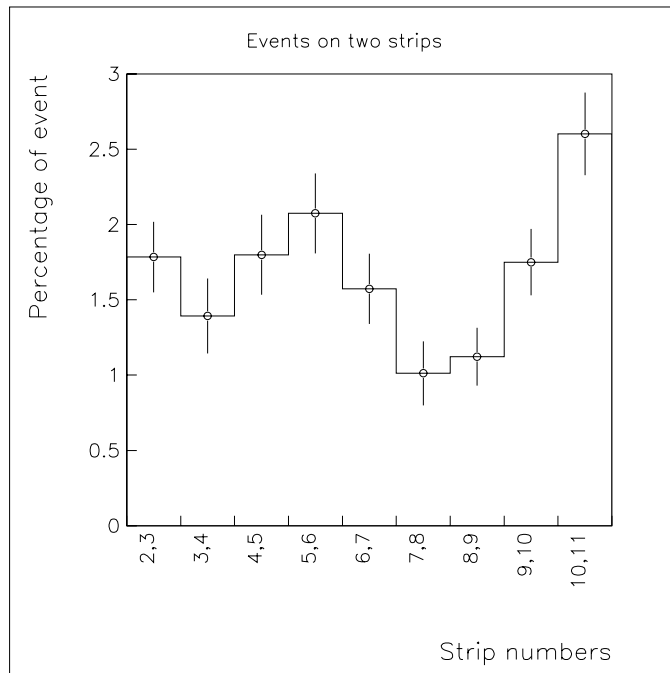


Figure 5.7: Events detected on two adjacent strips.

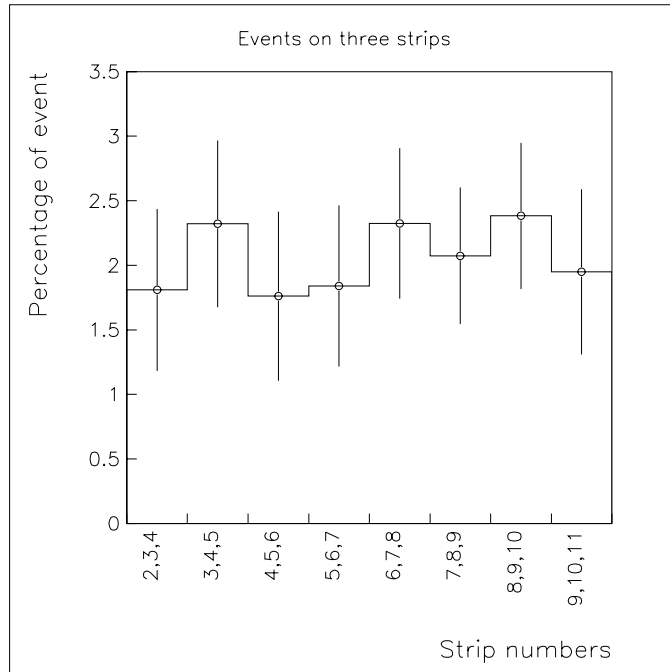


Figure 5.8: Events detected on three adjacent strips.

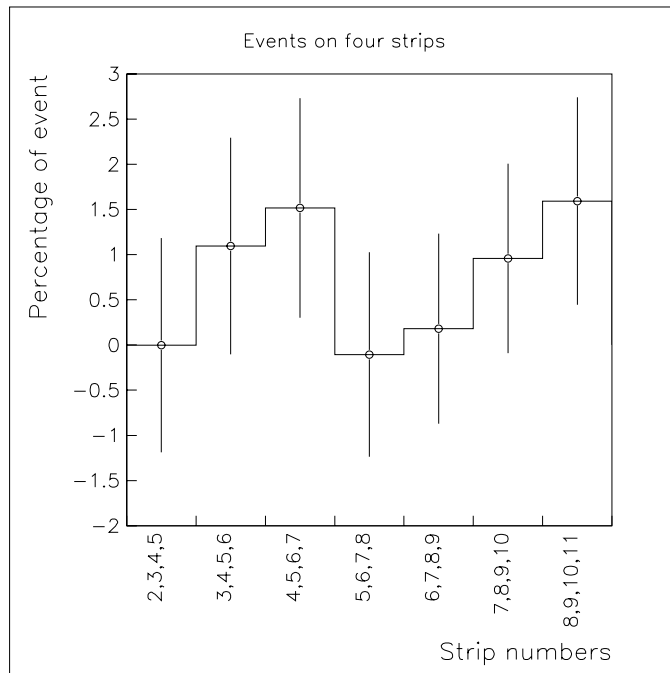


Figure 5.9: Events detected on four adjacent strips.

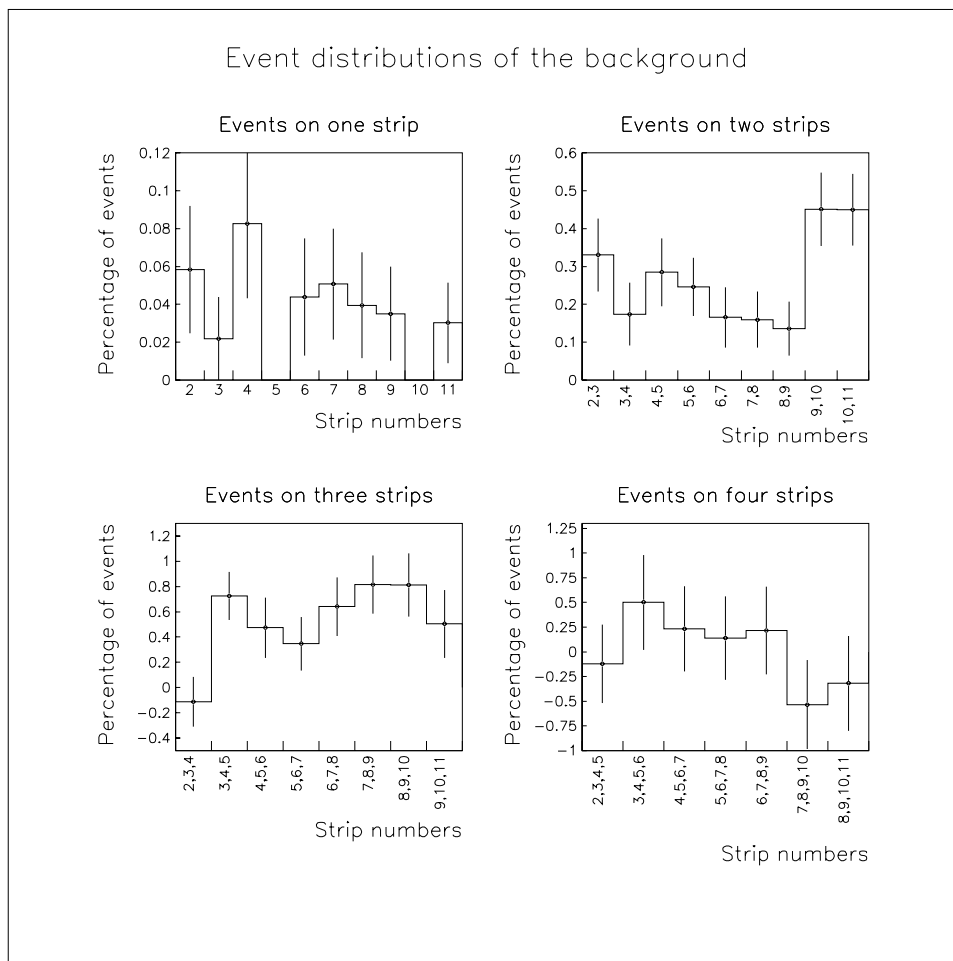


Figure 5.10: Event distributions of the noise on the strips.

Chapter 6

Conclusions

This work has established, that signals are well measurable in a drift chamber as the one described in Chapter 1. The 70 keV electrons emitted from the source (see Figure 5.2) are almost all collected on the strips (see Figure 5.5). With the construction of a similar drift chamber with a bigger drift space of about 10 cm one should be able to measure the Lorentz angle calculated in Chapter 1. The results suggest that a slit should be inserted in such a drift chamber in order to have a clear localized signal: this will facilitate the measurement of the Lorentz angle.

Detailed measurements of the events on the strips and measurements of the event size (from 1 strip up to 4 strips) have been made. These measurements, in the case of one and two strips soldered in the central channel, show a structure in the events distribution on the strips. In the case of three and four strips soldered in the central channel, on the contrary, the measurements show a uniform distribution of the events on the strips. The results of these measurements are presented in Chapter 5.

Bibliography

- [1] ICANOE proposal, CERN/SPSC 99-25, 1999.
- [2] ICARUS proposal, LNGS/CERN, 2001.
- [3] F.Sauli, Principle of operation of multiwire proportional and drift chambers, CERN 77-09 (1977).
- [4] The European Physical Journal, Review of Particle Physics, Springer, 2000 , equation (24.7).
- [5] Diploma Thesis of Marco Laffranchi, ETH Zuerich, September 2000.
- [6] Karlsruher Nukleidkarte, 5. Edition, 1981.
- [7] Private communication Zuxiang Dai, ETHZ, April 2002.
- [8] Diploma Thesis of Paolo Crivelli, ETH Zuerich, September 2001.
- [9] Private communication Marco Laffranchi, ETHZ, July 2002.

Acknowledgments

I would like to thank Prof. André Rubbia for giving me the possibility to make the diploma thesis in his group, and for all the advices he gave me. A special thanks to Dr. Andreas Badertscher for all his precious advices. A special thanks to Marco Laffranchi too, who helped me very much in all the stages of the diploma work, and taught me a lot of things. Last but not least I would like to thank Gustav Natterer, Leo Knecht, Rosa Bächli and Markus Bischofberger for their help.

Rigraziamenti

Vorrei inoltre ringraziare di cuore i miei genitori per avermi sostenuto moralmente ed economicamente e per avermi permesso di arrivare fino a qui. Un ringraziamento speciale per Matteo, che mi ha sopportato anche nei momenti di maggiore stress. Grazie anche a tutti gli amici per i bellissimi momenti passati assieme durante questi cinque anni di studio.